

Probing the Electronic and Structural Properties of the Niobium Trimer Cluster and Its Mono- and Dioxides: Nb_3O_n^- and Nb_3O_n ($n = 0-2$)[†]

Hua-Jin Zhai,[‡] Bin Wang,[§] Xin Huang,^{*,§} and Lai-Sheng Wang^{*,‡}

Department of Physics, Washington State University, 2710 University Drive, Richland, Washington 99354, Chemical & Materials Sciences Division, Pacific Northwest National Laboratory, MS K8-88, Post Office Box 999, Richland, Washington 99352, Department of Chemistry, Fuzhou University, Fuzhou, Fujian 350108, P. R. China, and State Key Laboratory of Structural Chemistry, Fuzhou, Fujian 350002, P. R. China

Received: November 11, 2008; Revised Manuscript Received: January 07, 2009

We report a photoelectron spectroscopy and density functional theory (DFT) study on the electronic and structural properties of Nb_3^- , Nb_3O^- , Nb_3O_2^- , and the corresponding neutrals. Well-resolved photoelectron spectra are obtained for the anion clusters at different photon energies and are compared with DFT calculations to elucidate their structures and chemical bonding. We find that Nb_3^- possesses a C_{2v} (3A_2) structure, and Nb_3 is a scalene C_s ($^2A''$) triangle. Both Nb_3O^- and Nb_3O are found to have C_{2v} structures, in which the O atom bridges two Nb atoms in a Nb_3 triangle. The ground-state of Nb_3O_2^- is found surprisingly to be a low symmetry C_1 (1A) structure, which contains a bridging and a terminal O atom. Molecular orbital analyses are carried out to understand the structures and bonding of the three clusters and provide insights into the sequential oxidation from Nb_3^- to Nb_3O_2^- . The terminal Nb=O unit is common in niobia catalysts, and the Nb_3O_2^- cluster with a Nb=O unit may be viewed as a molecular model for the catalytic sites or the initial oxidation of a Nb surface.

1. Introduction

Niobium oxides have been actively pursued for catalytic applications over the past two decades and have been found to possess many different catalytic properties.¹ As active species, niobium oxides catalyze a range of important chemical reactions such as selective hydrocarbon oxidation, NO_x reduction for exhaust gas purification, and photocatalytic splitting of water. As a catalyst support, niobium oxides can enhance catalytic activity and selectivity due to strong metal–support interactions. More intriguingly, niobium oxides are also known to be a strong catalytic promoter. Understanding the various roles that niobium oxides can play in catalysis at the molecular level can help the design of better catalysts, but it is a challenging task because of the complexity of real world catalytic systems.

Gas-phase cluster studies provide a valuable means to model catalytic sites and give mechanistic insights.² In the present work, we study the niobium trimer cluster and its initial oxidation by one and two oxygen atoms. Small niobium clusters and niobium oxide clusters have been studied in a number of previous experimental^{3–12} and theoretical works.^{7,10,13–15} Nb_xO_y^- cluster anions have been shown to activate methanol and ethanol,⁸ in which the Nb=O double bond is deemed to be essential. The Nb_3O cluster in its various charge states has been characterized via ZEKE⁷ and high-resolution photoelectron spectroscopy (PES).⁹ Its ionization potential, electron affinity, and ground-state vibrational frequencies are measured to be 5.526 eV,⁷ 1.393 eV,⁹ 710 cm^{-1} (ref 9), and 320 cm^{-1} ,⁷ respectively. Infrared spectroscopy on Nb_xO_y^+ cations has

allowed structural assignment for a number of clusters, such as Nb_2O_6^+ , Nb_3O_8^+ , $\text{Nb}_4\text{O}_{10}^+$, and $\text{Nb}_4\text{O}_{11}^+$.¹⁰ To the best of our knowledge, no prior work has been reported on the Nb_3O_2 cluster, although PES¹⁶ and Raman^{4a} studies have been reported for the bare Nb_3^- and Nb_3 clusters, respectively, and all $\text{Nb}_3^{+/0/-}$ species have been studied theoretically by a number of groups.^{17–22}

We are interested in developing cluster models^{23,24} for early transition metal oxide catalysts and in elucidating new types of chemical bonding in novel oxide clusters.^{25–27} In a previous study,²⁶ we found the first δ -aromatic molecule in the Ta_3O_3^- cluster, which possesses a planar D_{3h} structure. Recently, we have characterized Ta_3^- (D_{3h} , $^5A_1'$),²⁸ which is connected to Ta_3O_3^- by adding three bridging O atoms. To compare the oxide clusters of Nb vs Ta, we conducted a preliminary survey of a series of Nb_3O_n^- clusters and found some significant differences between the two systems. The current report focuses on a combined PES and density functional theory (DFT) study on the electronic and structural properties of Nb_3O_n^- ($n = 0-2$). The concerted experimental and computational results establish the ground-state structures for Nb_3O_n^- ($n = 0-2$). Our findings on Nb_3^- and Nb_3O^- are consistent with previous reports. However, Nb_3O_2^- is found to be quite unusual, in which the second O atom is shown to prefer a terminal site, in contrast to the first O atom which prefers a bridging site. Molecular orbital (MO) analyses are used to understand the sequential oxidation from Nb_3^- to Nb_3O_2^- and the unusual Nb_3O_2^- ground-state structure.

2. Experimental and Computational Methods

2.1. Photoelectron Spectroscopy. The experiment was carried out using a magnetic-bottle PES apparatus equipped with a laser vaporization supersonic cluster source, details of which have been described elsewhere.²⁹ Briefly, the Nb_3O_n^- ($n = 0-2$)

[†] Part of the “George C. Schatz Festschrift”.

* Corresponding authors. E-mails: xhuang@fzu.edu.cn; ls.wang@pnl.gov.

[‡] Department of Physics, Washington State University, and Chemical & Materials Sciences Division, Pacific Northwest National Laboratory.

[§] Department of Chemistry, Fuzhou University, and State Key Laboratory of Structural Chemistry.

clusters were produced by laser vaporization of a niobium disk target using a pure He carrier gas. The trace amount of oxygen in the carrier gas or residual oxygen on the target surface was sufficient to produce abundant Nb_3O^- and Nb_3O_2^- clusters for the current study, whereas the use of a He/O₂ mixed carrier gas was found to result in highly oxidized clusters. The anion clusters were analyzed using a time-of-flight mass spectrometer, and the Nb_3O_n^- ($n = 0-2$) clusters were each mass-selected and decelerated before being photodetached. Four detachment photon energies were used in the present work: 532 nm (2.331 eV), 355 nm (3.496 eV), 266 nm (4.661 eV), and 193 nm (6.424 eV). Effort was made to choose colder clusters for photo-detachment, which has proved essential for obtaining high-quality PES data.³⁰ Photoelectrons were collected at nearly 100% efficiency by the magnetic bottle and analyzed in a 3.5 m long electron flight tube. PES spectra were calibrated using the known spectra of Au^- and Rh^- , and the energy resolution of the apparatus was $\Delta E/E \sim 2.5\%$, i.e., ~ 25 meV for 1 eV electrons.

2.2. Density Functional Calculations. The theoretical calculations were performed at the DFT level using the B3LYP hybrid functional.³¹⁻³³ A number of structural candidates including different spin states and initial structures were evaluated, and the search for the global minima was performed using analytical gradients with the Stuttgart 14-valence-electron pseudopotentials and the valence basis sets^{34,35} augmented with two *f*-type and one *g*-type polarization functions [$\zeta(f) = 0.261, 0.970; \zeta(g) = 0.536$] for Nb as recommended by Martin and Sundermann³⁶ and the aug-cc-pVTZ basis set for oxygen.^{37,38} Scalar relativistic effects, i.e., the mass velocity and Darwin effects, were taken into account via the quasi-relativistic pseudopotentials. Vibrational frequency calculations were performed at the same level of theory to verify the nature of the stationary points.

Vertical electron detachment energies (VDEs) were calculated using the generalized Koopmans' theorem by adding a correction term to the eigenvalues of the anion.³⁹ The correction term was estimated by $\delta E = E_1 - E_2 - \epsilon_{\text{HOMO}}$, where E_1 and E_2 are the total energies of the anion and neutral, respectively, in their ground states at the anion equilibrium geometry and ϵ_{HOMO} corresponds to the eigenvalue of the highest occupied molecular orbital (HOMO) of the anion. All the calculations were performed with the Gaussian03 software package.⁴⁰ Three-dimensional contours of the molecular orbitals were visualized using the VMD software.⁴¹

3. Experimental Results

The photoelectron spectra of Nb_3O_n^- at different photon energies are shown in Figures 1-3 for $n = 0-2$, respectively. The observed transitions are labeled with letters, and the measured adiabatic detachment energies (ADEs) and VDEs are given in Table 1 for all three species.

3.1. Nb_3^- . The 532 nm spectrum of Nb_3^- (Figure 1a) reveals two well-defined bands (X and A). The X band (VDE: 1.07 eV) represents the ground-state transition; it is much narrower and more intense than band A. Since no vibrational structures are resolved for band X, the ground-state ADE is evaluated by drawing a straight line along the leading edge of band X and then adding the instrumental resolution to the intersection with the binding energy axis. Although this is an approximate procedure, we are able to obtain a consistent ADE from the well-defined spectral onsets of band X at different photon energies. The ADE thus evaluated for Nb_3^- is 1.03 ± 0.02 eV, which represents the electron affinity of neutral Nb_3 .

At 355 nm (Figure 1b), the A band with a VDE of 1.80 eV is more intense, but it is clearly seen to have a shoulder on the

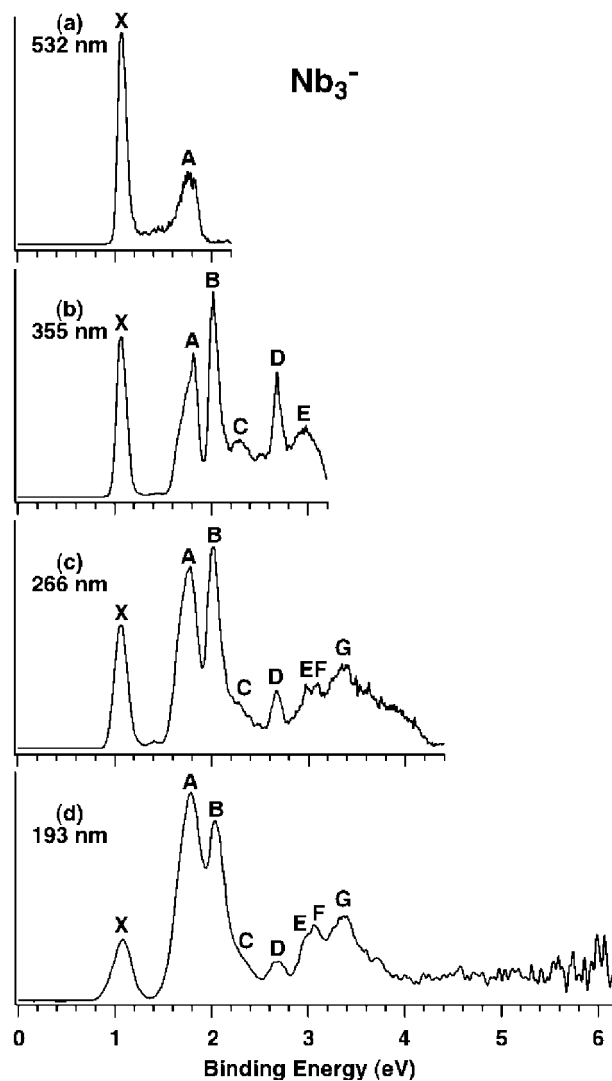


Figure 1. Photoelectron spectra of Nb_3^- at (a) 532 nm (2.331 eV), (b) 355 nm (3.496 eV), (c) 266 nm (4.661 eV), and (d) 193 nm (6.424 eV).

low binding energy side, suggesting overlapping electronic transitions. A relatively intense and sharp band B is seen at a VDE of 2.02 eV. Higher binding energy features in the 355 nm spectrum become more congested, but three bands can still be identified: C at 2.30 eV, D at 2.68 eV, and E at 2.98 eV. The band D is quite sharp, whereas bands C and E are relatively weak and broad. The 355 nm spectrum is consistent with a previous PES work at 4.0 eV photon energy,¹⁶ except that the bands C, D, and E are better resolved in the current data. At higher photon energies (Figure 1 c, d), only a broad band G is observed at the higher binding energy side, in addition to a resolved band F closely adjacent to band E. No more detachment features are observed beyond 4 eV in the 193 nm spectrum (Figure 1d).

3.2. Nb_3O^- . The 532 nm spectrum of Nb_3O^- (Figure 2a) reveals the ground-state detachment transition (X) with discernible vibrational structures, which are consistent with prior high-resolution ZEKE and PES studies ($\nu_1 = 710 \pm 15$ cm^{-1} and $\nu_3 = 320 \pm 1$ cm^{-1}).^{7,9} The 0-0 transition yields an electron affinity for Nb_3O as 1.40 ± 0.02 eV, which agrees well with the more accurate value (1.393 ± 0.006 eV) obtained from the previous high-resolution PES study.⁹ At 355 nm (Figure 2b), a series of weak bands (a, b, c, A) are observed followed by a sharp and intense band B and a weak band C. Both bands A

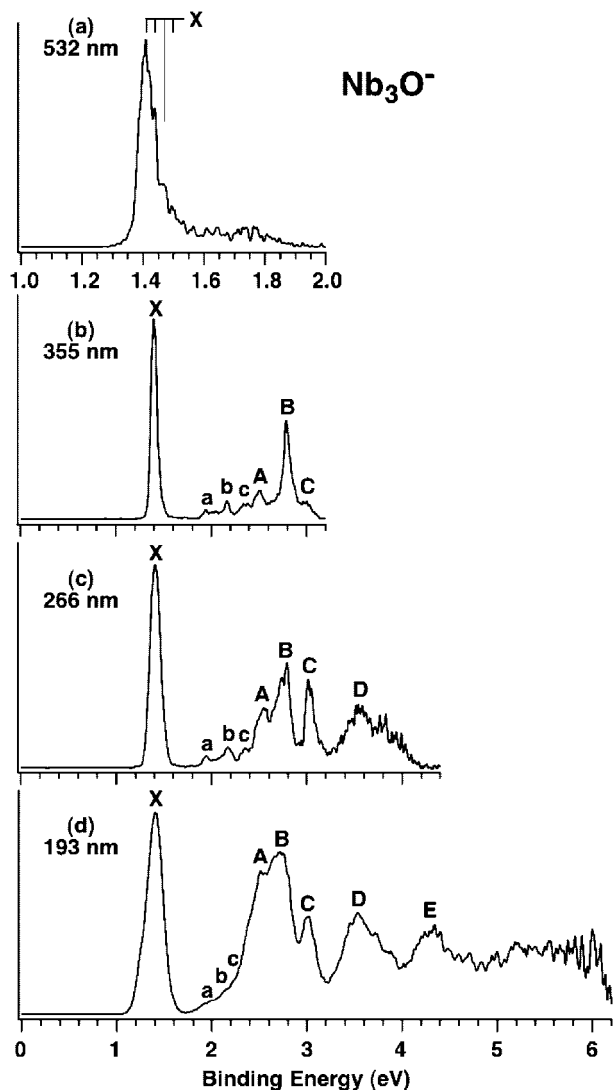


Figure 2. Photoelectron spectra of Nb_3O^- at (a) 532 nm, (b) 355 nm, (c) 266 nm, and (d) 193 nm. Note the different binding energy scale in (a), where the vertical lines represent vibrational structures.

and C become more intense in the 266 and 193 nm spectra. However, the bands (a, b, c) remain very weak also in the higher photon energy spectra. The bands a and b are also observed in the previous high-resolution PES study at 2.54 eV.⁹ As will be shown below, these weak features, a–c, do not correspond to one-electron transitions. They are likely due to multielectron (shakeup) transitions, consistent with their weak intensities. At high photon energies (Figure 2 c, d), two broad bands D and E are observed.

3.3. Nb_3O_2^- . The 355 nm spectrum of Nb_3O_2^- (Figure 3a) reveals two partially overlapping bands X and A, followed by a broad band B. A weak feature (X') at 1.33 eV is also observed, likely due to a minor isomer of Nb_3O_2^- because it becomes negligible in the high photon energy spectra. The onset of band X defines an electron affinity of 1.98 ± 0.05 eV for Nb_3O_2 . The onset of X' yields a very low electron affinity for the minor isomer of Nb_3O_2 as 1.29 ± 0.05 eV. The 266 nm spectrum (Figure 3b) reveals a new band C at 3.40 eV. At 193 nm (Figure 3c), a gap is observed beyond band C, followed by a broad band D centered around ~ 5 eV, which probably contains multiple unresolved detachment transitions. The PES bands for Nb_3O_2^- are all broad, suggesting a floppy Nb_3O_2^- or a large anion-to-neutral geometrical change.

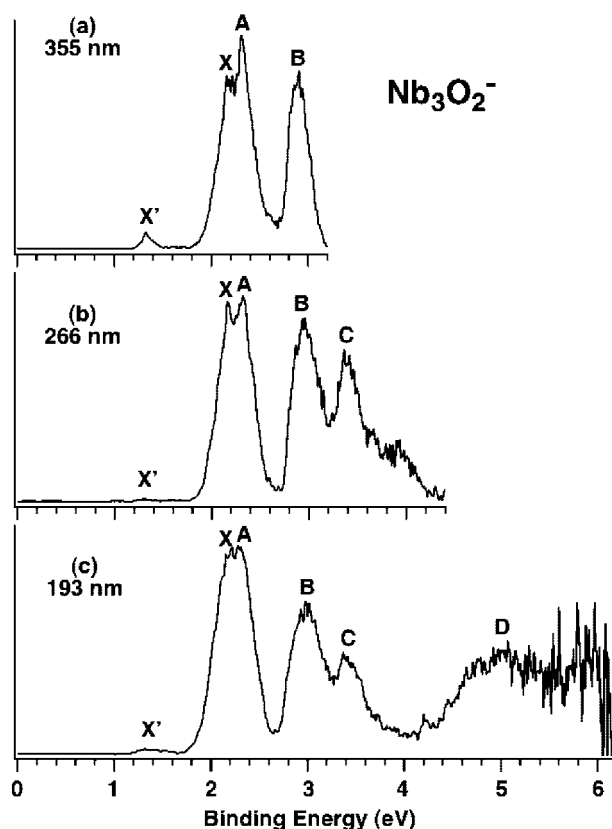


Figure 3. Photoelectron spectra of Nb_3O_2^- at (a) 355 nm, (b) 266 nm, and (c) 193 nm. The weak band X' at the low binding energy side is attributed to a minor isomer.

4. Theoretical Results

The optimized ground-state geometries of Nb_3O_n^- and Nb_3O_n ($n = 0-2$) and selected low-lying isomers are presented in Figures 4–6, and their calculated VDEs are compared with the experimental values in Tables 1 and 2. The simulated PES spectra from the lowest-energy structures are compared with experiment in Figure 7, where the simulations are done by fitting the distribution of calculated VDEs with unit-area Gaussian functions of 0.1 eV width. All other optimized geometries along with their relative energies are collected in Figures S1–S6 (Supporting Information), and all coordinates are given in Table S1 (Supporting Information).

4.1. Nb_3^- and Nb_3 . Similar to our recent study on Ta_3^- and Ta_3 ,²⁸ we considered four structures for the corresponding $\text{Nb}_3^{-/0}$ clusters with different spin multiplicities (Figures S1 and S2, Supporting Information): the equilateral triangle (D_{3h}), the isosceles triangle (C_{2v}) with two long and one short sides, the isosceles triangle (C_{2v}) with one long and two short sides, and the scalene triangle (C_s). A selected set of optimized low-lying structures along with their relative energies are shown in Figure 4. The ground state of Nb_3^- (Figure 4a) is an open-shell isosceles triangle (C_{2v} , 3A_2) with two long bonds (2.449 Å) and one short bond (2.152 Å), in agreement with previous theoretical studies.^{16,21} The equilateral triangle with D_{3h} symmetry ($^5A_1'$) is the second low-lying isomer 0.24 eV above the ground state for Nb_3^- (Figure 4b). Interestingly, we showed recently that the D_{3h} ($^5A_1'$) high spin structure is the ground state for the valent isoelectronic Ta_3^- cluster.²⁸ The structures and relative energies of other low-lying isomers are given in Figure S1 (Supporting Information).

The ground state of Nb_3 is a scalene triangle ($^2A''$) with C_s symmetry (Figure 4c), in agreement with a recent theoretical

TABLE 1: Experimental Adiabatic (ADE) and Vertical (VDE) Detachment Energies of Nb_3O_n^- ($n = 0-2$) and Comparison with the Calculated VDEs from the Lowest-Energy Structures of Nb_3^- (C_{2v} , 3A_2), Nb_3O^- (C_{2v} , 1A_1), and Nb_3O_2^- (C_1 , 1A)^a

	feature	ADE (exp) ^{b,c}	VDE (exp) ^b	channel ^d	VDE (theo)
Nb_3^-	X	1.03 (2)	1.07 (2)	$5a_1(\alpha)$	1.03
				$4a_1(\beta)$	1.43
	A			$2b_1(\beta)$	1.51
				$4a_1(\alpha)$	1.56
				$1b_2(\beta)$	1.66
				$2b_1(\alpha)$	1.74
				$3a_1(\beta)$	1.77
	B	2.02 (2)		$1a_2(\alpha)$	1.78
				$3a_1(\alpha)$	1.78
				$1b_2(\alpha)$	2.03
				$2a_1(\beta)$	2.51
	C	2.30 (5)		$1b_1(\beta)$	2.89
				$2a_1(\alpha)$	2.92
D	2.68 (2)		$1b_1(\alpha)$	3.00	
E	2.98 (4)		$1a_1(\beta)$	3.18	
F	3.08 (4)		$1a_1(\alpha)$	3.28	
			$2b_2$	1.19	
Nb_3O^-	X	1.40 (2) ^e	1.40 (2)		
	a ^f		1.94 (3)		
	b ^f		2.17 (3)		
	c ^f		2.36 (3)		
	A		2.52 (3)	$3a_1$	2.22
	B		2.78 (2)	$1a_2$	2.46
Nb_3O_2^-	C		3.02 (2)	$2a_1$	2.75
	D		3.55 (5)	$1b_2$	2.76
	E		4.30 (5)	$1b_1$	3.42
	X	1.98 (5)	2.19 (5)	$1a_1$	3.98 ^g
				$6a$	1.81
A		2.32 (2)	$5a$	1.89	
B		2.95 (5)	$4a$	2.20	
C		3.40 (5)	$3a$	2.78	
D		~ 4.4–5.5	$2a$	2.89	
X'	1.29 (5)	1.33 (2)	a	3.34	
			a	4.69 ^h	
			a	5.13 ^h	
			a	5.31 ^h	

^a All energies are in eV. ^b Numbers in the parentheses represent experimental uncertainty in the last digit. ^c Electron affinity of the neutral species. ^d The electron configurations for Nb_3^- (C_{2v} , 3A_2), Nb_3O^- (C_{2v} , 1A_1), and Nb_3O_2^- (C_s , 1A) anions are $1a_1^2 1b_1^2 2a_1^2 1b_2^2 3a_1^2 1a_2^2 1b_2^2 4a_1^2 5a_1^1$, $1a_1^2 1b_1^2 1b_2^2 2a_1^2 1a_2^2 3a_1^2 2b_2^2$, and $1a^2 2a^2 3a^2 4a^2 5a^2 6a^2$, respectively. ^e A more accurate electron affinity was reported previously, 1.393 ± 0.006 eV (ref 9). ^f Minor features, likely due to shakeup transitions. ^g Lowest binding energy O 2p transitions: 7.30 eV (b_1), 7.71 eV (a_1), and 7.86 eV (b_2). ^h Detachment from terminal O 2p based orbitals. The next lowest binding energy O 2p transitions from the bridging O atom: 6.72 eV (a), 7.12 eV (a), and 7.26 eV (a).

study.²² However, in several previous DFT studies,^{18–20} isosceles triangles have been reported to be the ground state. MRSDCI and DFT calculations were carried out on different electronic states of Nb_3 and Nb_3^- by Majumdar and Balasubramanian.^{21a} The DFT and MRSDCI results predicted the ground state of Nb_3^- as 1A_1 and 3A_2 , respectively, and also suggested that the ground state of Nb_3 is 2B_1 with C_{2v} symmetry at both MRSDCI and DFT levels. In our calculations, the corresponding doublet isosceles triangular structures of Nb_3 (2B_1 and 2A_2 ; Figure S2, Supporting Information) are transition states with imaginary frequencies ($-17i$ cm^{-1} for 2B_1 and $-28i$ cm^{-1} for 2A_2), which turn into the C_s (${}^2A''$) ground state upon optimization. A previous resonance Raman spectroscopy study^{3a} suggested that the ground state of the Nb_3 molecule has a nearly equilateral triangular

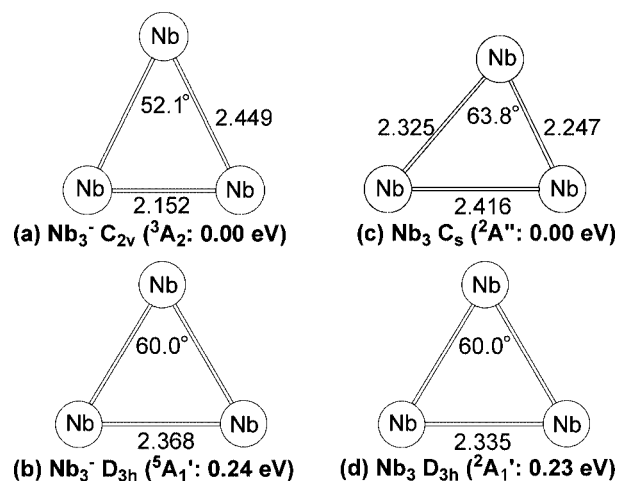


Figure 4. Calculated lowest-energy structures and selected low-lying isomers for Nb_3^- (a and b) and Nb_3 (c and d). Selected bond distances (Å) and bond angles ($^\circ$) are shown.

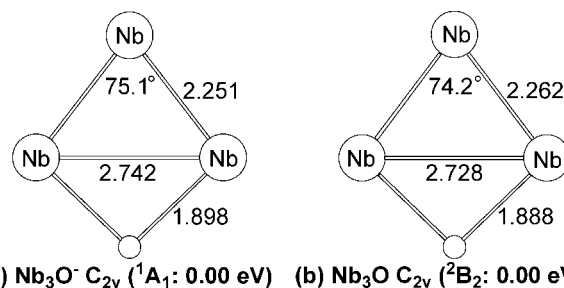


Figure 5. Calculated lowest-energy structures for (a) Nb_3O^- and (b) Nb_3O . Selected bond distances (Å) and bond angles ($^\circ$) are shown.

geometry (D_{3h}). However, we find that the D_{3h} (${}^2A_1'$) structure is a low-lying isomer 0.23 eV above the ground state (Figure 4d). Further theoretical calculations with more sophisticated methods may be necessary to resolve the true ground state of the $\text{Nb}_3^{-/0}$ clusters.

4.2. Nb_3O^- and Nb_3O . We optimized many structures and different spin states for Nb_3O^- (Figure S3, Supporting Information) and Nb_3O (Figure S4, Supporting Information), including planar and nonplanar structures with a bridging O, planar structures with a terminal O, and three-dimensional structures with the O atom capped on the top of a triangular Nb_3 cluster. The planar C_{2v} structure with a bridging O atom is found to be the overwhelmingly favorite for both Nb_3O^- and Nb_3O , as shown in Figure 5, in agreement with previous experimental and theoretical studies.^{7,9,15} The ground state of Nb_3O^- (Figure 5a) is found to be closed-shell (C_{2v} , 1A_1), and the closest isomer is a triplet (C_{2v} , 3B_2) 0.46 eV higher in energy (Figure S3, Supporting Information). The ground state of Nb_3O (Figure 5b) is a doublet (C_{2v} , 2B_2) with structural parameters very similar to those for the anion ground state. All other optimized isomers of the neutral cluster are significantly higher (>0.7 eV) in energy (Figure S4, Supporting Information).

4.3. Nb_3O_2^- and Nb_3O_2 . We optimized a variety of structures in search of the ground state for Nb_3O_2^- (Figure S5, Supporting Information) and Nb_3O_2 (Figure S6, Supporting Information). In contrast to the mono-oxides, many close-lying structures are found for the dioxide clusters, and selected low-lying isomers and their relative energies are shown in Figure 6. Most surprisingly, the ground state of Nb_3O_2^- (Figure 6a) is found to be a closed-shell C_1 (1A) structure with one bridging and one terminal O atom. Another similar C_1 (3A) structure with a triplet spin state (Figure 6b) is only 0.03 eV higher in energy,

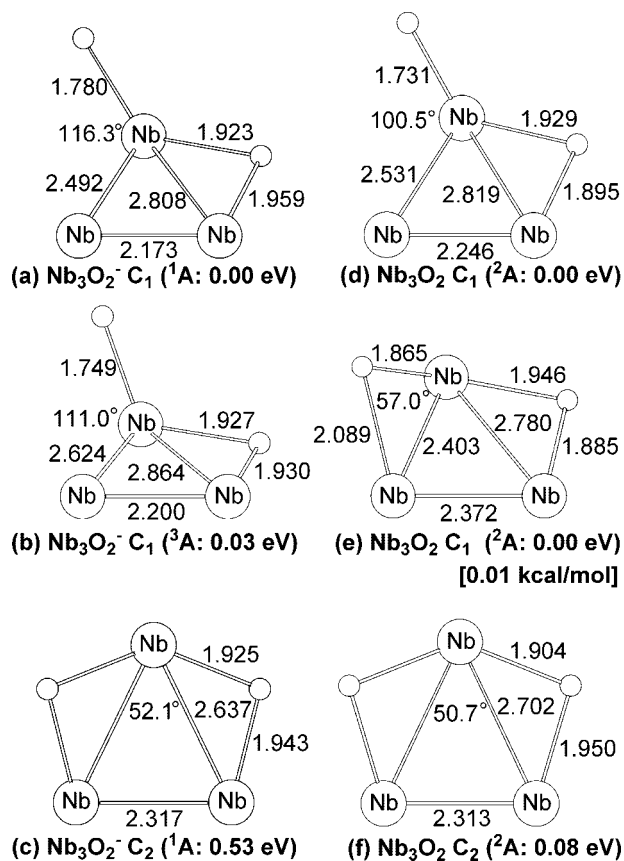


Figure 6. Calculated lowest-energy structures and selected low-lying isomers for Nb₃O₂⁻ (a–c) and Nb₃O₂ (d–f). Selected bond distances (Å) and bond angles (°) are shown.

TABLE 2: Comparison of First Experimental VDEs with Those Calculated from the Lowest-Energy Structures and Selected Low-Lying Isomers of Nb₃O_n⁻ (n = 0–2)^a

	VDE (exp) ^b	state	symmetry	ΔE ^c	VDE (theo)
Nb ₃ ⁻	1.07 (2)	³ A ₂	C _{2v}	0.00	1.03
		⁵ A ₁ '	D _{3h}	0.24	1.18
		³ B ₁	C _{2v}	0.27	0.74
		¹ A ₁ '	D _{3h}	0.30	0.80
Nb ₃ O ⁻	1.40 (2)	¹ A ₁	C _{2v}	0.00	1.19
		³ B ₂	C _{2v}	0.46	0.73
		³ A ₁	C _{2v}	0.49	0.72
		³ A ₂	C _{2v}	0.52	0.70
Nb ₃ O ₂ ⁻	2.19 (5)	¹ A	C ₁	0.00	1.81
		³ A	C ₁	0.03	1.74
		³ A	C ₁	0.17	1.41
		¹ A	C ₁	0.40	1.14
		¹ A	C ₂	0.53	1.33

^a All energies are in eV. ^b Numbers in the parentheses represent experimental uncertainty in the last digit. ^c Relative energy with respect to the lowest-energy structure.

competing for the ground state. A C₁ (³A) structure with two bridging O atoms is only 0.17 eV above the ground state (Figure S5, Supporting Information), whereas a C₂ (¹A) dibridged structure is 0.53 eV above the ground state (Figure 6c). The ground state of Nb₃O₂ (Figure 6d) is found to be similar to that of the anion with a terminal O atom. However, a C₁ (²A) dibridged structure (Figure 6e) is only 0.01 kcal/mol higher in energy, essentially degenerate to the ground state. A C₂ (²A) dibridged structure (Figure 6f) is also very close to the ground state only 0.08 eV higher in energy. All other structures are at least 0.2 eV higher in energy, as given in detail in Figure S6 (Supporting Information).

5. Comparison Between Experiment and Theory

5.1. Nb₃⁻. The Nb₃⁻⁰ clusters appear to be highly challenging species for quantum chemistry as discussed in section 4.1. We will attempt to qualitatively interpret our PES spectra with the aid of the DFT calculations. The C_{2v} ground state of Nb₃⁻ possesses a valence electron configuration of 1a₁²1b₁²2a₁²1b₂²3a₁²2b₁²4a₁²1a₂¹5a₁¹ with two unpaired electrons, giving rise to the triplet spin state (³A₂). The nine valence MOs lead to 16 one-electron detachment channels; the computed VDEs for all the one-electron transitions are compared with the experimental data in Table 1. The overall pattern of the simulated PES spectrum is in remarkable agreement with the experimental spectrum, as shown in Figure 7. The deepest valence MO is the 1a₁ orbital, which gives rise to two detachment channels with calculated VDEs at 3.18 eV (β) and 3.28 eV (α) (Table 1). These should correspond to the observed band G at ~3.35 eV. Experimentally, there is no more detachment band beyond band G, which is born out from our calculations. Clearly, many of the observed PES bands contain multiple detachment transitions (Figure 7 and Table 1). We note that in a previous joint theoretical and PES study on small Nb_n⁻ clusters the calculated detachment transitions from a triplet C_{2v} Nb₃⁻ were found to agree well with the experimental spectrum, consistent with the current finding.^{16,42} Our first VDE upon photodetachment from the singly occupied 5a₁ HOMO is predicted to be 1.03 eV, which is in excellent agreement with the experimental value of 1.07 eV (Table 1). The removal of the 5a₁ electron leads to the doublet ground state of Nb₃, which distorts into a C_s structure (²A'', Figure 4c). Thus, the first detachment band (Figure 1) of Nb₃⁻ should contain a complicated vibrational structure.

5.2. Nb₃O⁻. The current DFT calculations show that the ground state of Nb₃O⁻ and Nb₃O consists of a Nb₃ triangle with a bridging O atom (Figure 5), consistent with previous spectroscopic and theoretical studies on these species.^{7,9,15} The geometry change between the ground states of Nb₃O⁻ and Nb₃O is minor, which agrees with the sharp ground-state PES band dominated by the 0–0 transition (see Figure 2 and ref 9). The ground-state electron configuration of Nb₃O⁻ is closed-shell (¹A₁): 1a₁²1b₁²1b₂²2a₁²1a₂²3a₁²2b₂². The calculated VDEs (Table 1) and simulated PES spectrum (Figure 7) for Nb₃O⁻ agree well with the experimental data. The VDE of the ground-state transition is predicted as 1.19 eV, which is lower than the experimental value (1.40 eV, Table 1) by ~0.2 eV. The previous spectrum⁹ yielded an electron affinity of 1.393 ± 0.006 eV for Nb₃O. As seen from Table 1 and Figure 7, the calculated VDEs seem to be lower by 0.2 eV systematically than experiment for every detachment channel.

Our calculations show that there are no one-electron detachment transitions in the energy range between 1.19 and 2.22 eV, i.e., between the bands X and A (Figure 7c). Therefore, the observed weak features (a, b, c) are likely due to multielectron (shakeup) transitions, which have been observed quite definitively in a number of cluster systems previously.^{26,28,43} These weak features could also be due to low-lying isomers, but they can be ruled out on the basis of both energetic argument and the simulated PES spectra (Figure 8). The closest lying isomer is 0.46 eV higher in energy (Figure S3, Supporting Information), which is too high to allow any significant population under our current experimental conditions. Figure 8 compares the simulated PES spectra of three higher-energy isomers, which all have a low binding energy ground-state detachment feature. Such a feature is not observed in the experimental PES spectra (Figure 2).

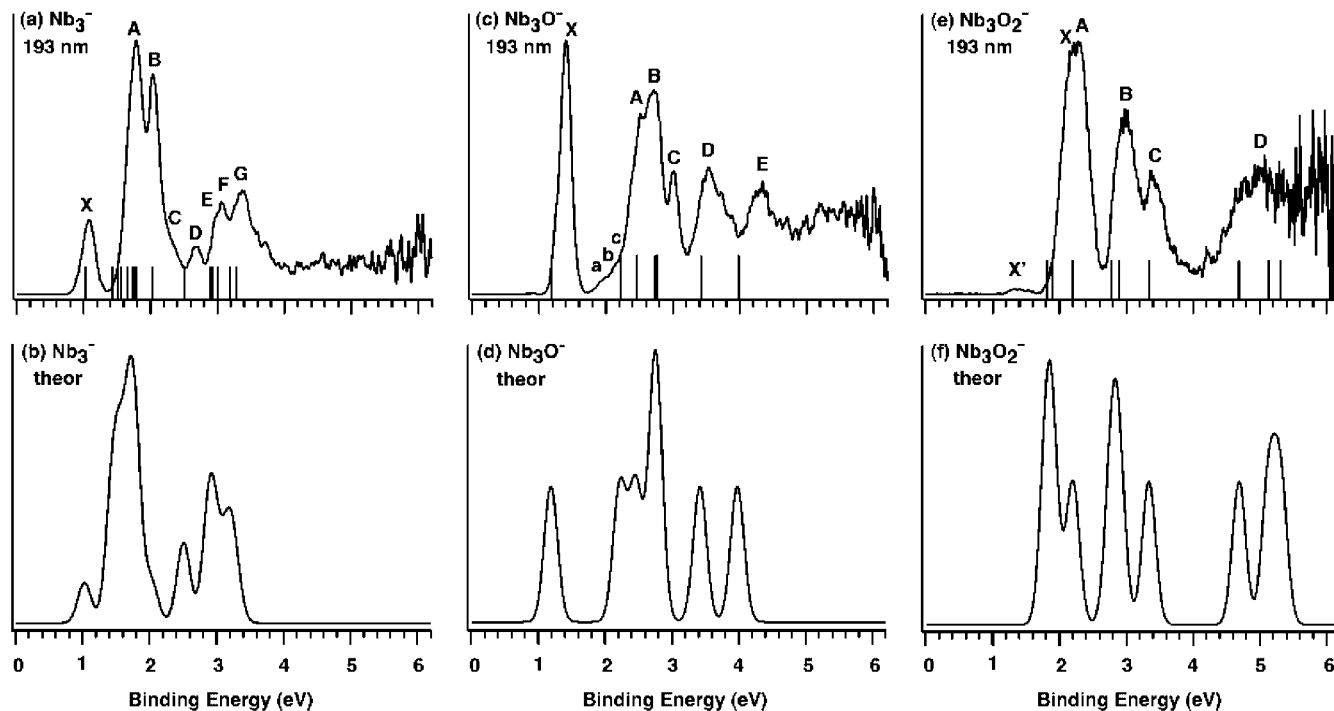


Figure 7. Comparison of the 193 nm photoelectron spectra of Nb_3O_n^- ($n = 0-2$) (a, c, and e) with those simulated from their lowest-energy C_{2v} (3A_2), C_{2v} (1A_1), and C_1 (1A) structures, respectively (b, d, and f). The vertical bars in (a), (c), and (e) represent the calculated VDEs from the lowest-energy anion structures. The simulated PES spectra are constructed by fitting the distribution of the calculated VDE values with unit-area Gaussian functions of 0.1 eV width.

The shakeups involve most likely detachment of a HOMO electron and simultaneous excitation of the remaining electron in the HOMO to a higher unoccupied MO. We calculated the excitation energies from the HOMO of Nb_3O^- to its LUMO, LUMO+1, and LUMO+2 using two theoretical methods (ΔSCF and TD-DFT), as shown in Table S2 in the Supporting Information. While the excitation energies strongly depend on the level of theory, the calculated transition energies support our interpretation that the weak features come from shakeup processes. For example, the measured excitation energy from X to a is 0.54 eV (Table 1), which is well in line with the calculated excitation energy from the anion HOMO to LUMO (0.46 and 0.49 eV at the TD-DFT and ΔSCF level of theory, respectively; Table S2, Supporting Information). The observation of shakeup transitions indicates strong electron correlation effects in the Nb_3O^- anion.

5.3. Nb_3O_2^- . The potential energy surface of Nb_3O_2^- is much more complicated with several low-lying isomers (Figure 6 and Figure S5, Supporting Information). The ground state is found to be a C_1 (1A) isomer with a terminal O atom (Figure 6a), but there are four low-lying isomers within 0.5 eV of the ground state. Fortunately, all these isomers yield distinct simulated PES spectra (Figures 7f and 9), and the experimental spectra can thus serve as electronic fingerprints to assign the cluster structures. As shown in Table 1 and Figure 7f, the calculated VDEs and the simulated PES spectrum for the ground state C_1 (1A) structure are in excellent agreement with the experimental data, and it should be the dominant species observed. The predicted first and second VDEs, 6a (1.81 eV) and 5a (1.89 eV), are very close to each other and should correspond to the X band (VDE: 2.19 eV). The predicted VDE (2.20 eV) for the third detachment channel is in good agreement with band A (VDE: 2.32 eV). The VDEs for the fourth and fifth detachments, 3a (2.78 eV) and 2a (2.89 eV), are predicted to be close and should correspond to the broad band B at 2.95 eV. The sixth

detachment channel, 1a (3.34 eV), agrees well with the band C at 3.40 eV. The PES spectrum displays a large energy gap followed by a broad band D, which is also well reproduced from the simulated spectrum. The 1a to 6a orbitals, which are responsible for the lower binding energy features, are all Nb-derived MOs (see Figure 10). Higher binding energy features beyond 4.5 eV are due to detachment from O 2p-based MOs. Three such detachment transitions (VDEs: 4.69, 5.13, and 5.31 eV) are predicted in the D band region (Table 1 and Figure 7f). There are also quite significant structural changes from the ground state of Nb_3O_2^- (Figure 6a) to that of the neutral (Figure 6d), consistent with the broad PES spectral features.

However, both the first VDE (Table 2) and the simulated PES spectra (Figure 9) for the other four low-lying isomers do not agree with the PES spectra of Nb_3O_2^- . The low-lying C_1 (3A) triplet isomer, which is only 0.03 eV above the ground state at the current level of theory, is expected to be populated in the experiment. The simulated spectrum of this isomer (Figure 9b) displays a low binding energy feature, which could be assigned to the weak X' feature observed experimentally. The higher binding energy features from this isomer are likely to be buried beneath the PES features from the ground-state isomer. Another isomer, which is 0.17 eV higher in energy, could also be the carrier for the X' band (Figure 9c). However, on energetic grounds, we tentatively assign the 0.03 eV isomer as the more likely candidate. Overall, the excellent agreement between the theory and the experiment for the ground-state isomer lends considerable credence to the unusual C_1 structure with a terminal O atom for Nb_3O_2^- (Figure 6a).

6. Discussion

6.1. Comparison of Nb_3^- vs Ta_3^- . In a combined PES and DFT study, we recently investigated the structure and bonding in Ta_3^- and found that it possesses a D_{3h} ($^5A_1'$) structure with a high spin quintet ground state.²⁸ More interestingly, we found

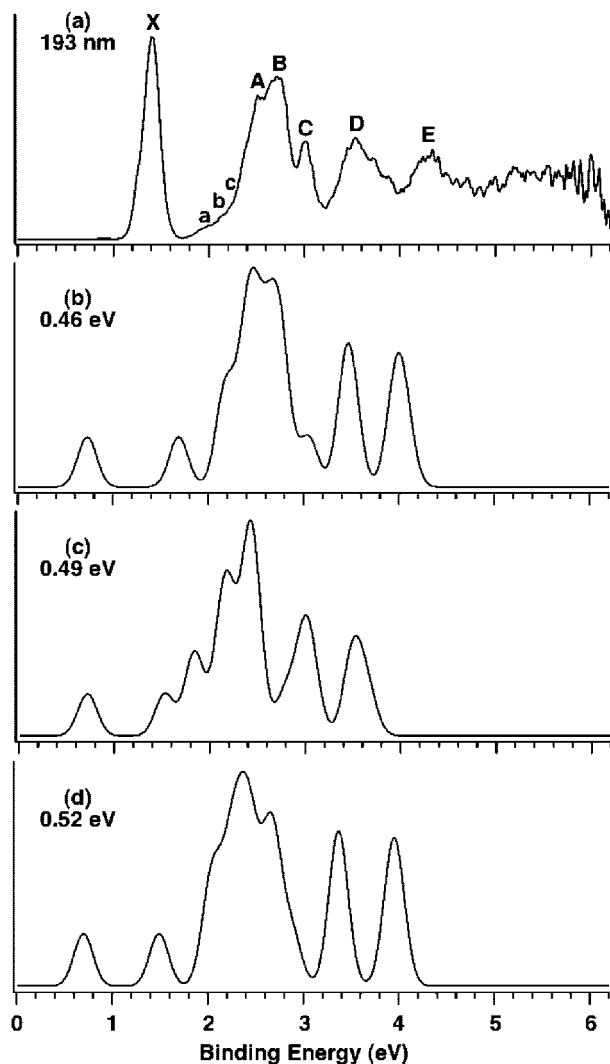


Figure 8. Comparison of the 193 nm PES spectrum of Nb₃O⁻ (a) with those simulated from three low-lying isomers (b–d), none of which matches the experimental data. The relative energies for the isomeric structures (see Table 2 and Figure S3, Supporting Information) with respect to the anion ground state are labeled.

that Ta₃⁻ is δ -aromatic with partial σ - and π -aromaticity. However, the current work shows that the ground state of the isoivalent Nb₃⁻ cluster has a C_{2v} (³A₂) structure with a lower spin multiplicity (Figure 4a). The corresponding D_{3h} quintet state for Nb₃⁻ is a higher-energy isomer (Figure 4b) and is not observed experimentally. Indeed, the PES spectra of Nb₃⁻ and Ta₃⁻ are quite different, reflecting the different electronic and atomic structures in their ground states. These observations suggest that δ -aromaticity, which is favored in the D_{3h} structure, is not strong in Nb₃⁻, most likely due to its weaker d–d bonding relative to that in Ta₃⁻. Their neutral ground states are also very different. The ground state of Nb₃ has a low-spin C_s (²A'') structure (Figure 4c), while two high-spin states, C_{2v} (⁴A₁) and D_{3h} (⁶A₁'), are nearly degenerate for Ta₃, competing for its ground state. The scalene triangular structure for Nb₃ is also quite unusual,²² which again is likely a result of the weaker d–d bonding.

6.2. Molecular Orbital Analyses and Sequential Oxidation. The electron affinities in the Nb₃O_n (*n* = 0–2) series exhibit a monotonic increase as a function of O, 1.03 eV for Nb₃, 1.40 eV for Nb₃O, and 1.98 eV for Nb₃O₂. This trend is consistent with our previous studies of other metal oxide clusters,

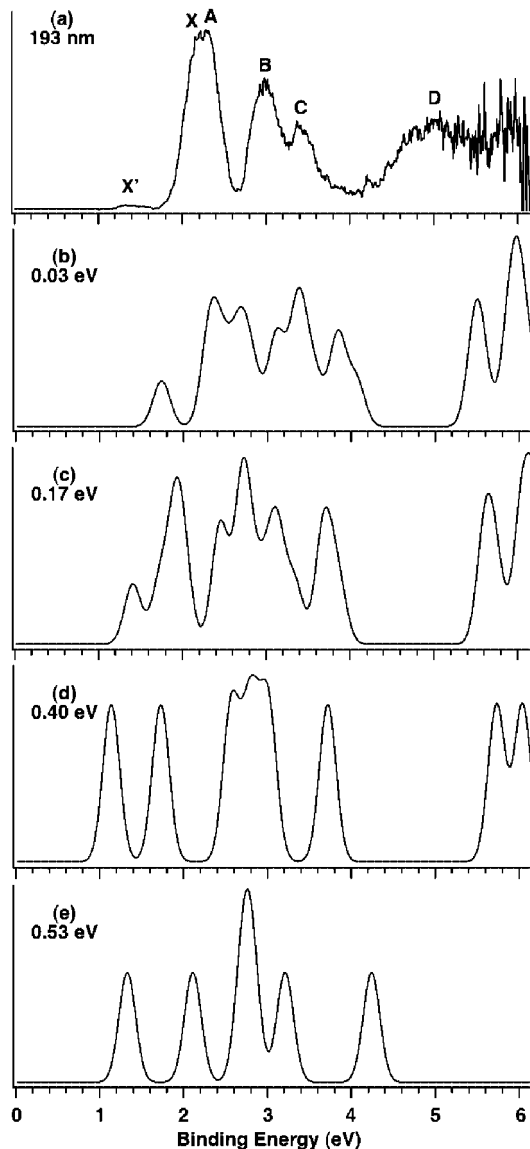


Figure 9. Comparison of the 193 nm PES spectrum of Nb₃O₂⁻ (a) with those simulated from four low-lying isomers (b–e). The relative energies for the isomeric structures (see Table 2 and Figure S5, Supporting Information) with respect to the anion ground state are labeled.

suggesting a sequential oxidation of the metal cluster.⁴⁴ This can be seen more clearly from the MO pictures, shown in Figure 10. Niobium has an electron configuration of 4d⁴5s¹. The 16 valence electrons in Nb₃⁻ (C_{2v}, ³A₂) occupy nine MOs (Figure 10a) with two half-filled orbitals, resulting in the triplet ground state. These Nb s/d-based MOs possess relatively low electron binding energies and are all observed experimentally (Table 1 and Figure 7a,b).⁴⁵ In Nb₃O⁻ (Figure 10b), there are only 14 electrons occupying 7 Nb s/d-based MOs because two of the Nb electrons are transferred to O. Two more electrons are transferred to O in Nb₃O₂⁻, which only possesses 12 s/d electrons (Figure 10c). Detachment features for the Nb s/d-based MOs always occur at lower binding energies, whereas those from O 2p are at higher binding energies usually beyond 5 eV, as shown in Figure 7e, f. The sequential oxidation is expected to continue with additional O atoms until Nb₃O₈⁻, which should possess three Nb(5+) centers with a very high electron binding energy. Our preliminary results show that Nb₃O₈⁻ has an electron binding energy larger than 5.5 eV.

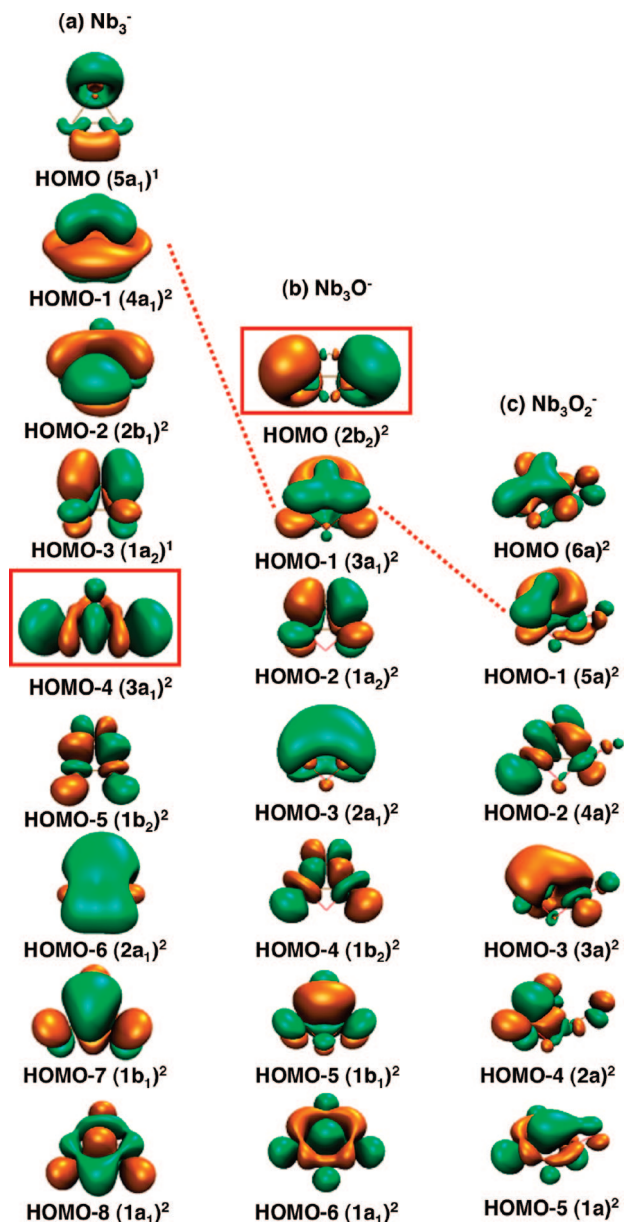


Figure 10. Valence molecular orbital pictures for the Nb-derived orbitals for the Nb_3O_n^- ($n = 0-2$) ground states: Nb_3^- ($C_{2v}, {}^3A_2$), Nb_3O^- ($C_{2v}, {}^1A_1$), and Nb_3O_2^- ($C_1, {}^1A$). The red squares denote MOs from which two Nb electrons are transferred to O 2p upon sequential oxidation. The dashed lines trace the δ -orbitals in the series.

6.3. Nb_3O_2^- : Terminal vs Bridging Oxygen Atom. The C_1 (1A) ground-state structure of Nb_3O_2^- with a terminal O atom is remarkable, in which every atom is unique and the three Nb atoms have different oxidation states: 0, +1, and +3. One would have guessed a dibridged structure, but they are all higher-energy isomers (Figure S5, Supporting Information). Why does the second O atom prefer a terminal position? Why does the terminal oxygen prefer to bind to the Nb site that is already bonded to a bridging oxygen? We can answer these questions and understand the unusual structure and bonding of Nb_3O_2^- by examining the MOs of Nb_3O^- , as shown in Figure 10b. The HOMO ($2b_2$) of Nb_3O^- is primarily an antibonding orbital of Nb 5s character, which has the highest electron density on the two Nb atoms bonded to the first O atom. The HOMO is well separated from the other 4d-based MOs, as seen in Figure 7c, d. A second bridging O atom is expected to interact mainly with the HOMO-2 ($1a_2$), which is much lower in energy and is not favored. Thus, the second O atom primarily interacts with the HOMO, forming the unusual terminal Nb=O unit. In fact, one can find all the remaining MOs of Nb_3O^- in the MOs of Nb_3O_2^- (Figure 10c). In contrast, our preliminary PES data show that the isoelectronic Ta_3O^- , which has the same C_{2v} (1A_1) ground-state as and a bonding pattern similar to Nb_3O^- , has a significantly smaller energy gap between its $1a_2$ orbital and the $2b_2$ HOMO. Consequently, its $1a_2$ orbital becomes competitive energetically to interact with the second O atom, resulting in a dibridged ground state for Ta_3O_2^- .

There is spectroscopic evidence for the terminal O atom in Nb_3O_2^- . Figures 7e and f show three detachment features from O 2p-based orbitals, corresponding to the broad D band in the PES spectrum. These O 2p detachment channels seem to have rather low binding energies (~ 5 eV). We have shown previously that the O 2p MOs for bridging O atoms tend to occur at higher electron binding energies. For example, the 193 nm PES spectrum of Nb_3O^- does not show an O 2p band at ~ 5 eV, and our DFT calculations suggest that its first O 2p-based MO has a detachment energy of 7.3 eV (Figure 11a). Our MO analyses confirm that the three low binding energy O 2p detachment channels in Nb_3O_2^- indeed originate from the terminal O atom (Figure 11 b–d), whereas the first O 2p detachment band from the bridging O atom is at a higher binding energy (Figure 11e). Due to their different binding energies, the terminal and bridging O atoms should exhibit distinct chemical reactivities. The terminal Nb=O is common on the surface of niobium oxides and is suggested to play an

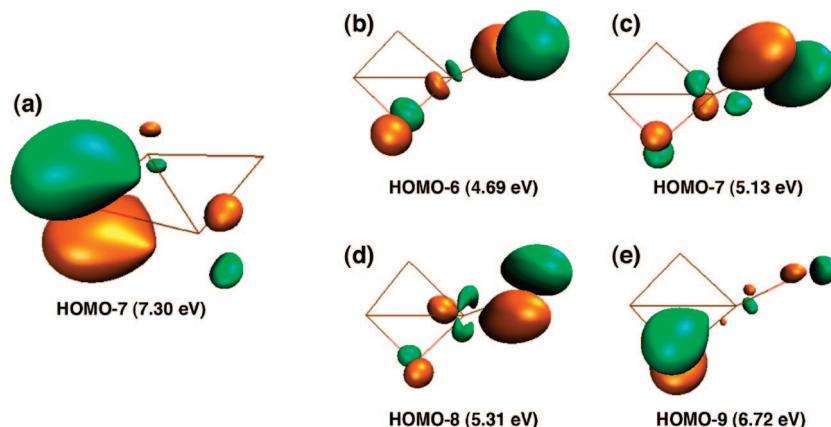


Figure 11. Pictures for selected O 2p-derived molecular orbitals for Nb_3O^- (a) and Nb_3O_2^- (b–e). The corresponding calculated vertical detachment energies are shown in parentheses. Note that the O 2p orbitals from the terminal O atom (b–d) exhibit significantly lower electron binding energies than those from the bridging O atom (a and e).

important role in the catalytic activities of niobia catalysts.⁴⁶ What is surprising is the early appearance of the terminal O atom because Nb_3O_2^- is metal-rich. Hence, the evolution from Nb_3^- to Nb_3O^- to Nb_3O_2^- may even be considered as molecular models for mechanistic understanding of the initial oxidation of Nb surfaces.⁴⁷

7. Conclusions

Photoelectron spectroscopy and DFT calculations are used to investigate the electronic and structural properties of Nb_3^- , Nb_3O^- , Nb_3O_2^- , and their neutrals. Well-resolved PES spectra are obtained for the anions and used to compare with the DFT calculations to elucidate the structures and bonding in the three clusters. Electron affinities are shown to increase with the degree of oxidation from 1.03 eV for Nb_3 to 1.40 eV for Nb_3O to 1.98 eV for Nb_3O_2 . Extensive DFT calculations are performed to locate the ground states and low-lying isomers for Nb_3O_n^- and Nb_3O_n ($n = 0-2$). The ground-state structures for Nb_3O_n^- ($n = 0-2$) are shown to be C_{2v} (3A_2), C_{2v} (1A_1), and C_1 (1A), respectively. The low-spin C_{2v} (3A_2) ground state for Nb_3^- is different from the high-spin D_{3h} ($^5A_1'$) ground state for the isoelectronic Ta_3^- .²⁸ The C_1 (1A) structure for Nb_3O_2^- is quite unexpected, which consists of a bridging and a terminal O atom. Molecular orbital analyses are carried out to understand the chemical bonding in the three clusters and provide insight into the sequential oxidation from Nb_3^- to Nb_3O_2^- .

Acknowledgment. The experimental work was supported by the Chemical Sciences, Geosciences, and Biosciences Division, Office of Basic Energy Sciences, U.S. Department of Energy (DOE), under grant No. DE-FG02-03ER15481 (catalysis center program) and performed at the W. R. Wiley Environmental Molecular Sciences Laboratory, a national scientific user facility sponsored by DOE's Office of Biological and Environmental Research and located at Pacific Northwest National Laboratory, operated for DOE by Battelle. X.H. gratefully acknowledges support from the Natural Science Foundation of China (20641004 and 20771026) and the Natural Science Foundation of Fujian Province of China (No. 2008J0151).

Supporting Information Available: Alternative optimized structures (Figures S1–S6) and their Cartesian coordinates (Table S1) for Nb_3O_n^- and Nb_3O_n ($n = 0-2$) and calculated excitation energies from the HOMO of the Nb_3O^- (C_{2v} , 1A_1) anion ground state to its LUMO, LUMO+1, and LUMO+2 using two theoretical methods (Table S2). This material is available free of charge via the Internet at <http://pubs.acs.org>.

References and Notes

- (1) For selected reviews, see: (a) Nowak, I.; Ziolk, M. *Chem. Rev.* **1999**, *99*, 3603. (b) Ziolk, M. *Catal. Today* **2003**, *78*, 47. (c) Tanabe, K. *Catal. Today* **2003**, *78*, 65.
- (2) For a recent review, see: Böhme, D. K.; Schwarz, H. *Angew. Chem., Int. Ed.* **2005**, *44*, 2336.
- (3) (a) Morse, M. D. *Chem. Rev.* **1986**, *86*, 1049. (b) Loh, S. K.; Lian, L.; Armentrout, P. B. *J. Am. Chem. Soc.* **1989**, *111*, 3167. (c) Knickelbein, M. B.; Yang, S. H. *J. Chem. Phys.* **1990**, *93*, 5760.
- (4) (a) Wang, H. M.; Craig, R.; Haouari, H.; Liu, Y. F.; Lombardi, J. R.; Lindsay, D. M. *J. Chem. Phys.* **1996**, *105*, 5355. (b) Aydin, M.; Lombardi, J. R. *Int. J. Mass Spectrom.* **2004**, *235*, 91.
- (5) Song, L.; Eychmüller, A.; St.Pierre, R. J.; El-Sayed, M. A. *J. Phys. Chem.* **1989**, *93*, 2485.
- (6) (a) Sigsworth, S. W.; Castleman, A. W., Jr. *J. Am. Chem. Soc.* **1992**, *114*, 10471. (b) Deng, H. T.; Kerns, K. P.; Castleman, A. W., Jr. *J. Phys. Chem.* **1996**, *100*, 13386. (c) Zemski, K. A.; Justes, D. R.; Bell, R. C.; Castleman, A. W., Jr. *J. Phys. Chem. A* **2001**, *105*, 4410. (d) Zemski, K. A.;

- Justes, D. R.; Castleman, A. W., Jr. *J. Phys. Chem. A* **2001**, *105*, 10237.
- (e) Justes, D. R.; Moore, N. A.; Castleman, A. W., Jr. *J. Phys. Chem. B* **2004**, *108*, 3855.
- (7) (a) Yang, D. S.; Zgierski, M. Z.; Rayner, D. M.; Hackett, P. A.; Martinez, A.; Salahub, D. R.; Roy, P. N.; Carrington, T., Jr. *J. Chem. Phys.* **1995**, *103*, 5335. (b) Athanassenas, K.; Kreisle, D.; Collings, B. A.; Rayner, D. M.; Hackett, P. A. *Chem. Phys. Lett.* **1993**, *213*, 105.
- (8) (a) Jackson, P.; Fisher, K. J.; Willett, G. D. *Int. J. Mass Spectrom.* **2000**, *197*, 95. (b) Jackson, P.; Fisher, K. J.; Willett, G. D. *Chem. Phys.* **2000**, *262*, 179.
- (9) Green, S. M. E.; Alex, S.; Fleischer, N. L.; Millam, E. L.; Marcy, T. P.; Leopold, D. G. *J. Chem. Phys.* **2001**, *114*, 2653.
- (10) Fielicke, A.; Meijer, G.; von Helden, G. *J. Am. Chem. Soc.* **2003**, *125*, 3659.
- (11) Molek, K. S.; Jaeger, T. D.; Duncan, M. A. *J. Chem. Phys.* **2005**, *123*, 144313.
- (12) Dong, F.; Heinbuch, S.; He, S. G.; Xie, Y.; Rocca, J. J.; Bernstein, E. R. *J. Chem. Phys.* **2006**, *125*, 164318.
- (13) Sambrano, J. R.; Andres, J.; Beltran, A.; Sensato, F.; Longo, E. *Chem. Phys. Lett.* **1998**, *287*, 620.
- (14) Martinez, A.; Calaminici, P.; Koster, A. M.; Salahub, D. R. *J. Chem. Phys.* **2001**, *114*, 819.
- (15) Calaminici, P.; Flores-Moreno, R.; Koster, A. M. *J. Chem. Phys.* **2004**, *121*, 3558.
- (16) (a) Kietzmann, H.; Morenzin, J.; Bechthold, P. S.; Gantefor, G.; Eberhardt, W.; Yang, D. S.; Hackett, P. A.; Fournier, R.; Pang, T.; Chen, C. F. *Phys. Rev. Lett.* **1996**, *77*, 4528. (b) Kietzmann, H.; Morenzin, J.; Bechthold, P. S.; Gantefor, G.; Eberhardt, W. *J. Chem. Phys.* **1998**, *109*, 2275. (c) Fournier, R.; Pang, T.; Chen, C. F. *Phys. Rev. A* **1998**, *57*, 3683.
- (17) Sellers, H. *J. Phys. Chem.* **1990**, *94*, 1338.
- (18) Goodwin, L.; Salahub, D. R. *Phys. Rev. A* **1993**, *47*, R774.
- (19) Grönbeck, H.; Rosén, A. *Phys. Rev. B* **1996**, *54*, 1549.
- (20) Fowler, J. E.; García, A.; Ugalde, J. M. *Phys. Rev. A* **1999**, *60*, 3058.
- (21) (a) Majumdar, D.; Balasubramanian, K. *J. Chem. Phys.* **2003**, *119*, 12866. (b) Majumdar, D.; Balasubramanian, K. *J. Chem. Phys.* **2001**, *115*, 885.
- (22) (a) Dryza, V.; Addicoat, M. A.; Gascooke, J. R.; Buntine, M. A.; Metha, G. F. *J. Phys. Chem. A* **2008**, *112*, 5582. (b) Addicoat, M. A.; Buntine, M. A.; Yates, B.; Metha, G. F. *J. Comput. Chem.* **2008**, *29*, 1497.
- (23) Zhai, H. J.; Döbler, J.; Sauer, J.; Wang, L. S. *J. Am. Chem. Soc.* **2007**, *129*, 13270.
- (24) (a) Zhai, H. J.; Kiran, B.; Cui, L. F.; Li, X.; Dixon, D. A.; Wang, L. S. *J. Am. Chem. Soc.* **2004**, *126*, 16134. (b) Huang, X.; Zhai, H. J.; Waters, T.; Li, J.; Wang, L. S. *Angew. Chem., Int. Ed.* **2006**, *45*, 657. (c) Zhai, H. J.; Wang, L. S. *J. Am. Chem. Soc.* **2007**, *129*, 3022. (d) Zhai, H. J.; Li, S. G.; Dixon, D. A.; Wang, L. S. *J. Am. Chem. Soc.* **2008**, *130*, 5167.
- (25) Huang, X.; Zhai, H. J.; Kiran, B.; Wang, L. S. *Angew. Chem., Int. Ed.* **2005**, *44*, 7251.
- (26) Zhai, H. J.; Averkiev, B. B.; Zubarev, D. Yu.; Wang, L. S.; Boldyrev, A. I. *Angew. Chem., Int. Ed.* **2007**, *46*, 4277.
- (27) Zubarev, D. Yu.; Averkiev, B. B.; Zhai, H. J.; Wang, L. S.; Boldyrev, A. I. *Phys. Chem. Chem. Phys.* **2008**, *10*, 257.
- (28) Wang, B.; Zhai, H. J.; Huang, X.; Wang, L. S. *J. Phys. Chem. A* **2008**, *112*, 10962.
- (29) (a) Wang, L. S.; Cheng, H. S.; Fan, J. *J. Chem. Phys.* **1995**, *102*, 9480. (b) Wang, L. S.; Wu, H. *Advances in Metal and Semiconductor Clusters, Vol. 4, Cluster Materials*; Duncan, M. A., Ed.; JAI Press: Greenwich, CT, 1998; pp 299–343.
- (30) (a) Wang, L. S.; Li, X. *Clusters and Nanostructure Interfaces*; Jena, P., Khanna, S. N., Rao, B. K., Eds.; World Scientific: NJ, 2000; pp 293–300. (b) Akola, J.; Manninen, M.; Hakkinen, H.; Landman, U.; Li, X.; Wang, L. S. *Phys. Rev. B* **1999**, *60*, R11297. (c) Wang, L. S.; Li, X.; Zhang, H. F. *Chem. Phys.* **2000**, *262*, 53. (d) Zhai, H. J.; Wang, L. S.; Alexandrova, A. N.; Boldyrev, A. I. *J. Chem. Phys.* **2002**, *117*, 7917.
- (31) Becke, A. D. *J. Chem. Phys.* **1993**, *98*, 1372.
- (32) Lee, C.; Yang, W.; Parr, R. G. *Phys. Rev. B* **1988**, *37*, 785.
- (33) Stephens, P. J.; Devlin, F. J.; Chabalowski, C. F.; Frisch, M. J. *J. Phys. Chem.* **1994**, *98*, 11623.
- (34) Andrae, D.; Haeussermann, U.; Dolg, M.; Stoll, H.; Preuss, H. *Theor. Chim. Acta* **1990**, *77*, 123.
- (35) Küchle, W.; Dolg, M.; Stoll, H.; Preuss, H. *Pseudopotentials of the Stuttgart/Dresden Group 1998*, revision August 11, 1998; <http://www.theochem.uni-stuttgart.de/pseudopotentiale>.
- (36) Martin, J. M. L.; Sundermann, A. *J. Chem. Phys.* **2001**, *114*, 3408.
- (37) Dunning, T. H., Jr. *J. Chem. Phys.* **1989**, *90*, 1007.
- (38) Kendall, R. A.; Dunning, T. H., Jr.; Harrison, R. J. *J. Chem. Phys.* **1992**, *96*, 6796.
- (39) Tozer, D. J.; Handy, N. C. *J. Chem. Phys.* **1998**, *109*, 10180.
- (40) Frisch, M. J.; Trucks, G. W.; Schlegel, H. B.; Scuseria, G. E.; Robb, M. A.; Cheeseman, J. R.; Montgomery, J. A., Jr.; Vreven, T.; Kudin, K. N.;

Burant, J. C.; Millam, J. M.; Iyengar, S. S.; Tomasi, J.; Barone, V.; Mennucci, B.; Cossi, M.; Scalmani, G.; Rega, N.; Petersson, G. A.; Nakatsuji, H.; Hada, M.; Ehara, M.; Toyota, K.; Fukuda, R.; Hasegawa, J.; Ishida, M.; Nakajima, T.; Honda, Y.; Kitao, O.; Nakai, H.; Klene, M.; Li, X.; Knox, J. E.; Hratchian, H. P.; Cross, J. B.; Bakken, V.; Adamo, C.; Jaramillo, J.; Gomperts, R.; Stratmann, R. E.; Yazyev, O.; Austin, A. J.; Cammi, R.; Pomelli, C.; Ochterski, J. W.; Ayala, P. Y.; Morokuma, K.; Voth, G. A.; Salvador, P.; Dannenberg, J. J.; Zakrzewski, V. G.; Dapprich, S.; Daniels, A. D.; Strain, M. C.; Farkas, O.; Malick, D. K.; Rabuck, A. D.; Raghavachari, K.; Foresman, J. B.; Ortiz, J. V.; Cui, Q.; Baboul, A. G.; Clifford, S.; Cioslowski, J.; Stefanov, B. B.; Liu, G.; Liashenko, A.; Piskorz, P.; Komaromi, I.; Martin, R. L.; Fox, D. J.; Keith, T.; Al-Laham, M. A.; Peng, C. Y.; Nanayakkara, A.; Challacombe, M.; Gill, P. M. W.; Johnson, B.; Chen, W.; Wong, M. W.; Gonzalez, C.; Pople, J. A. *Gaussian03*; revision D. 01; Gaussian, Inc.: Wallingford, CT, 2004.

(41) VMD (Visual Molecular Dynamics). Humphrey, W.; Dalke, A.; Schulten, K. *J. Mol. Graphics* **1996**, *14*, 33.

(42) Arguably the singlet state of Nb_3^- may be competitive. However, the VDE for the singlet state from the current DFT calculations deviates substantially from the experiment (Table 2). In addition, the VDE pattern for the singlet state also disagrees with the PES spectrum (ref 16a). The assignment of a singlet ground state for Nb_3^- in ref 21a is “not unambiguous” as those authors noted.

(43) (a) Zhai, H. J.; Wang, L. S.; Alexandrova, A. N.; Boldyrev, A. I.; Zakrzewski, V. G. *J. Phys. Chem. A* **2003**, *107*, 9319. (b) Zhai, H. J.; Bürgel, C.; Bonacic-Koutecky, V.; Wang, L. S. *J. Am. Chem. Soc.* **2008**, *130*, 9156.

(44) (a) Wang, L. S.; Wu, H.; Desai, S. R. *Phys. Rev. Lett.* **1996**, *76*, 4853. (b) Wang, L. S.; Wu, H.; Desai, S. R.; Lou, L. *Phys. Rev. B* **1996**, *53*, 8028. (c) Wu, H.; Li, X.; Wang, X. B.; Ding, C. F.; Wang, L. S. *J. Chem. Phys.* **1998**, *109*, 449.

(45) Molecular orbital analysis (Figure 10) shows that the anion HOMO orbitals in Nb_3^- ($5a_1$, 81% 5s + 7% 4d) and Nb_3O^- ($2b_2$, 58% 5s + 26% 4d) show strong Nb 5s characters, whereas that in Nb_3O_2^- ($6a$, 70% 4d + 7% 5s) is primarily composed from Nb 4d orbitals. This is consistent with the observed pronounced photon energy dependence for Nb_3^- (Figure 1) and Nb_3O^- (Figure 2).

(46) Uhl, A.; Sainio, J.; Lahtinen, J.; Shaikhutdinov, S.; Freund, H. J. *Surf. Sci.* **2007**, *601*, 5605.

(47) (a) Franchy, R.; Bartke, T. U.; Gassmann, P. *Surf. Sci.* **1996**, *366*, 60. (b) An, B.; Fukuyama, S.; Yokogawa, K.; Yoshimura, M. *Phys. Rev. B* **2003**, *68*, 115423. (c) Arfaoui, I.; Cousty, J.; Guillot, C. *Surf. Sci.* **2004**, *557*, 119. (d) Kilimis, D. A.; Lekka, Ch. E. *Mater. Sci. Eng., B* **2007**, *144*, 27.

JP809945N